Journal of Sound and Vibration 586 (2024) 118497

Contents lists available at ScienceDirect

Journal of Sound and Vibration

journal homepage: www.elsevier.com/locate/jsvi

Stability analysis of multi-insert rotating boring bar with stiffness variation

Taha Gokulu [a,b], Fabrizio Defant [c], Paolo Albertelli [a,b,*]

[a] Mechanical Engineering Department, Politecnico di Milano, Via La Masa 1, 20156 Milano, Italy
[b] Consorzio MUSP, Piacenza, Italy
[c] R&D Department, Pama S.p.A, Viale del Lavoro 10, 38068 Rovereto TN, Italy

ARTICLE INFO

Keywords:
Rotating boring bar
Multi-insert tool
Chatter suppression
Stiffness variation

ABSTRACT

Manufacturing faces challenges in boring processes, critical for hole enlargement and finishing, due to low stiffness leading to static deflection and regenerative chatter. Stiffness variation has emerged as a promising solution for effectively suppressing chatter, while multi-insert rotating boring bars offer a viable approach to addressing static deflection in long and slender boring bars, enabling better tolerance with a large operational length-to-diameter ratio. However, integrating technological innovations to suppress chatter and prevent static deflection complicates the problem from a modeling and stability analysis perspective, making it challenging to find a comprehensive solution in the existing literature. This study explores the stability of multi-insert rotating boring bars with stiffness variation, providing insights into selecting optimal stiffness variation parameters. It introduces a novel extension of the multi-dimensional cutting force model to rotating boring tools with multiple inserts, employing the zero-order harmonic solution to analyze the stability of boring processes with time-varying dynamics. Experimental validation demonstrates the effectiveness of the proposed methodology, achieving 5 out of 6 matches in stability lobe diagrams for multi-insert rotating boring bars without stiffness variation. The model's comprehensiveness is further demonstrated by comparing the results with those of existing studies in the literature for single-insert stationary boring bars. In the case without stiffness variation, the model successfully reproduces 4 out of 5 operating points, and with stiffness variation, it accurately predicts all 5 operating points. Sensitivity analyses guide the selection of optimal stiffness variation parameters for effective chatter suppression, favoring moderate frequencies and up to a 30% amplitude ratio.

1. Introduction

Boring bars play a vital role in manufacturing processes, serving to enlarge, cut, and finish holes in workpieces such as bearing rings, gears, engine cylinders, hydraulic valve bodies, etc. ensuring that these workpieces have accurately sized and finished holes to meet expected specifications. The inherently low stiffness of long, slender boring bars utilized in deep-hole boring operations creates two major issues. Firstly, they are susceptible to regenerative chatter even at minimal cutting depths. Secondly, the precision of the machining is adversely affected by the static deflection of the boring bar.

The emergence of chatter vibrations due to the closed-loop interaction between the dynamic behavior of the mechanical structure and the machining process poses a significant challenge during boring operations. This can lead to poor surface quality, unacceptable

* Corresponding author at: Mechanical Engineering Department, Politecnico di Milano, Via La Masa 1, 20156 Milano, Italy.
E-mail addresses: taha.gokulu@musp.net (T. Gokulu), fabrizio.defant@pama.it (F. Defant), paolo.albertelli@polimi.it (P. Albertelli).

https://doi.org/10.1016/j.jsv.2024.118497
Received 22 December 2023; Received in revised form 26 April 2024; Accepted 6 May 2024
Available online 7 May 2024

dimensional inaccuracies, reduced tool life, and decreased productivity due to a low material removal rate. To suppress chatter and overcome these issues, researchers have explored various chatter suppression techniques, including passive, semi-active, and active methods. Takahashi et al. [1] proposed an anisotropic tool design for improved dynamic stiffness and stability in boring operations. Tang et al. [2] utilized piezoelectric patches to enhance stiffness, reducing vibration and expanding stability frontier in the stability lobe diagram which depicts the areas where cutting processes are stable or unstable, based on varying combinations of spindle speed ω and depth of cut a_p. Yuvaraju et al. [3] demonstrated increased stability in internal turning by utilizing a constrained layer damping (CLD) boring bar for vibration reduction, outperforming conventional boring bars. However, passive methods are limited in adapting to changing conditions, while semi-active and active approaches offer adaptability through adjustable elements and feedback control [4]. Saleh et al. [5] utilized a magnetorheological (MR) fluid damper to enhance boring process stability, demonstrating improved damping and stiffness, which increased the chatter-free stability limit. Altintas et al. [6] introduced a boring bar system with a tuned mass damper (TMD) for vibration absorption, featuring adjustable TMD heads for various bar lengths. Vashisht et al. [7] proposed an active control strategy employing a fractional-order PD^{λ} controller and an electromagnetic actuator for chatter mitigation. While experiments indicated reduced chatter, the model's dependence on accurate measurement and modeling of manufacturing inaccuracies restricts its feasibility in industrial scenarios. Despite the progress in chatter suppression technologies throughout the years, more work is required to find effective and feasible solutions for industrial applications, especially for large-scale boring machines. Modulating tool stiffness around a nominal value is an effective approach for chatter suppression in industrial settings. This technique alters the natural frequency of the structure through stiffness variation (SV), effectively disturbing the regeneration mechanism. It holds particular promise for machining processes with limited stiffness improvement options [8]. SV, adaptable as a semi-active or active approach, offers implementation flexibility. Li et al. [9] demonstrated the effectiveness of a dynamically variable stiffness absorber (DVA) for boring bars in reducing vibration. Mei et al. [8,10] used MR fluid to adjust stiffness and suppress chatter, evaluating stability enhancement through sensitivity analysis. However, stability lobe diagrams for different SV frequencies were estimated only by shifting the lobes in the frequency axis due to the natural frequency changes using the energy approach.

Stability analysis of boring process with SV involves the solution of time-periodic delayed differential equations (DDEs), which can be performed through methods such as the semi-discretization [11] and full-discretization [12]. Sun et al. [13] developed high-order full-discretization methods to study the stability of turning with SV and provided insights into the effects of SV amplitude and frequency parameters on the stability enhancement, but the methodology was only validated through time domain simulations. Defant et al. [14] introduced the Harmonic Solution (HS), an efficient approach to analyze the stability of both Linear time-invariant (LTI) and linear time-periodic (LTP) system dynamics, that can also deal with systems with arbitrary time-period-to-delay ratio (TPTDR) ratios, and is based on the generalized harmonic balance approach of Wereley et al. [15]. Originally developed for milling processes, this method has the potential to be applied to other machining operations with LTP dynamics due to its fast convergence and accurate results compared to semi-discretization [14]. In addition, it is also an accurate and efficient technique for conducting sensitivity analysis and optimization of SV parameters.

Performing boring operations on large and non-cylindrical workpieces can be challenging due to static deflection in long and slender boring bars. However, this issue can be overcome by using a multi-insert rotating boring bar while the workpiece remains stationary on a table. Symmetric placement of cutting inserts balances the static contributions of the cutting forces and enables better tolerance with a large operational length-to-diameter ratio, as well as improved cylindricity, which is crucial for workpieces that need to be both round and straight along their axis, such as sliding shafts and engine cylinders. In addition, using multiple inserts in a boring cutting head has the advantage of achieving a higher feed rate and a higher material removal rate compared to using a single insert, which leads to increased productivity for the machining center [16]. Atabey et al. [16–18] developed a model predicting cutting forces and uncut chip area configurations for different cutting conditions in boring processes with both single and multiple inserts. However, the study was focused on stationary boring bars, and limited by its exclusion of some tool angles. Budak et al. [19] proposed a multi-dimensional model for turning and stationary single-insert boring bars, considering tool angles. Chen et al. [20] modeled rotating single-insert boring bars, and Li et al. [21] extended it to stationary boring bars, comparing rotating and stationary tools. Wang et al. [22] used the multi-dimensional approach [19] for robotic boring bar processes, optimizing a robot's posture for increased stiffness. However, none of these studies focused on rotating boring bars with multiple inserts.

While multiple inserts in boring cutting tools offer productivity and precision advantages, their potential has not been adequately explored in existing literature through an analytical stability analysis. Technological advancements aimed at suppressing chatter and mitigating static deflection add complexity to this analysis, making it a challenging issue to address comprehensively in the literature. Therefore, there is a pressing need for further research on the analytical stability analysis of boring processes involving time-varying dynamic parameters and configurations, including rotating boring bars equipped with multiple cutting inserts. This study focuses on precisely this area to address the research gap. The contributions of this research are twofold. First, the multi-dimensional boring cutting force model developed by Budak et al. [19] and adopted to rotating boring bars by Wang et al. [22] has been extended to rotating boring bars with multiple inserts by summing the contributions of each insert to the total cutting force, considering the tool angles and orientation of the cutting insert. Second, the study by Defant et al. [14] on chatter stability analysis with the HS was extended and adapted to the boring process. These advancements lead to a deeper understanding of the complex nature of boring and provide valuable insights for machining practitioners and researchers. Experimental validation emphasized the efficacy of the proposed methodology in predicting stability lobe diagrams for multi-insert rotating boring bars without SV. The model's comprehensiveness was further demonstrated by comparison with findings from prior studies in the literature on single-insert stationary boring bars, encompassing cases with and without SV. The research also aimed to identify optimal parameters for SV in machining processes to achieve stability. The study conducted a sensitivity analysis, offering an alternative perspective to the

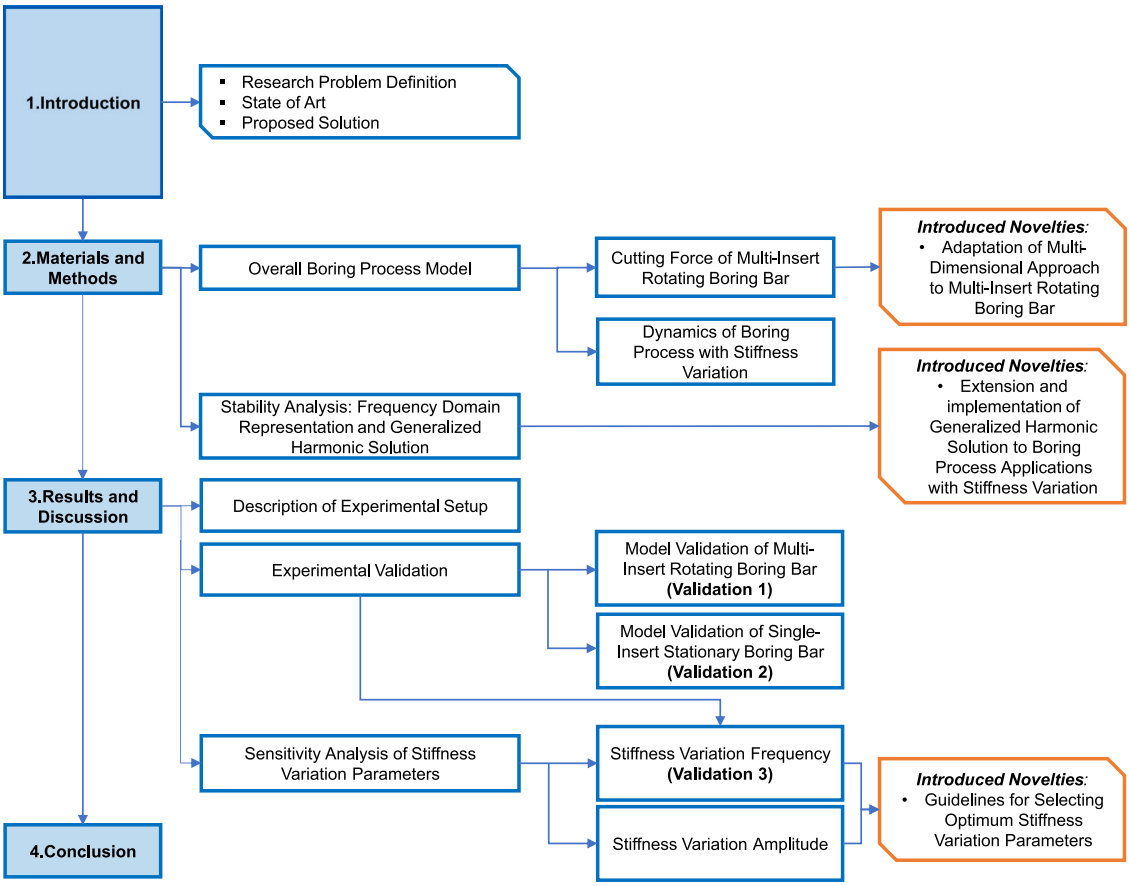

Fig. 1. Organization of the article.

insights presented by Sun et al. [13] and Mei et al. [8]. Specifically, the investigation reexamined the selection of SV parameters and their impact on stability enhancement, aiming to strengthen practical knowledge. Unlike prior studies that primarily focused on the influence of SV parameters on chatter suppression performance at a single operating point, this approach considered the stabilization effect across the speed axis of the stability lobe diagram. This nuanced perspective allowed for the assessment of the impact of SV parameters region by region, providing a more comprehensive understanding of their effects on stability.

This paper is structured as outlined below, with a schematic representation provided in Fig. 1. The cutting force model of a multi-insert rotating boring tool was introduced in Section 2, where the dynamics of the boring process with SV were thoroughly examined. The stability analysis was presented utilizing a frequency domain representation and HS. In Section 3, the description of the experimental setup employed in this study was provided. Furthermore, validation of the proposed dynamic model and stability analysis methodology was presented. This validation was achieved through experimental validation and a comparative analysis of the findings with relevant studies in the existing literature. Lastly, in Section 4, the procedure and the achieved results were summarized leading to the derivation of comprehensive conclusions.

2. Material and method

As illustrated in Fig. 1 within the context of Section 2, this section introduced the cutting force model for a rotating boring tool with multiple inserts. Following this, a comprehensive examination of the dynamics of the boring process with SV was presented. Subsequently, stability analysis was conducted with the HS.

2.1. Overall boring process model

2.1.1. Cutting force model of multi-insert rotating boring tool

According to Fig. 2, a stationary global coordinate frame (x , y , z) is set up at the rotation center of the boring bar, while a local coordinate frame (q_1 , q_2 , q_3) is established at the cutting edge of the insert as shown in Fig. 2(a). The local coordinate frame rotates along with the boring bar [22].

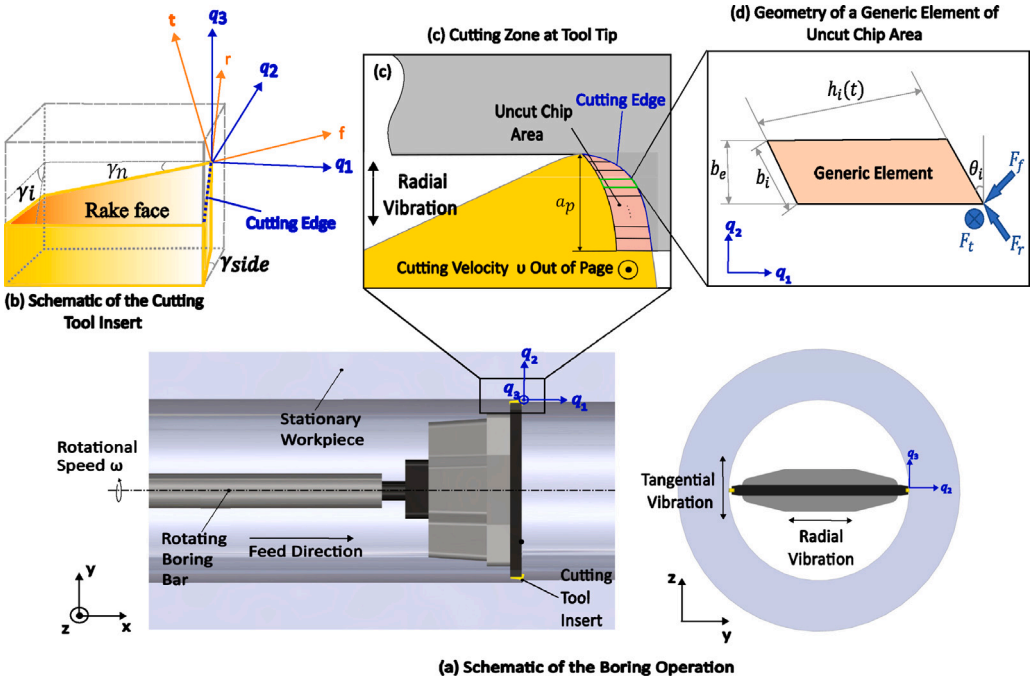

Fig. 2. Schematic illustration of the overall boring process.

An additional cartesian coordinate frame called a cutting coordinate frame (t , f , r) is established on the rake face of the cutting insert, as depicted in the accompanying Fig. 2(b). The tangential t and radial r axes of this coordinate frame are parallel to the cutting velocity v and cutting edge, respectively. Meanwhile, the feed f axis is positioned orthogonally to both t and r. The cutting force components in feed F_f, radial F_r, and tangential F_t directions can be projected into the local coordinate frame (q_1, q_2, q_3) knowing the angles of the cutting tool which are side cutting edge angle γ_{side}, inclination angle γ_i, and normal rake angle γ_n as follows [22],

$$\begin{Bmatrix} F_{q_1} \\ F_{q_2} \\ F_{q_3} \end{Bmatrix} = \delta \begin{Bmatrix} F_f \\ F_r \\ F_t \end{Bmatrix} \tag{1}$$

where

$$\delta = \begin{bmatrix} \cos(\gamma_n)\cos(\gamma_{\text{side}}) & -\cos(\gamma_i)\sin(\gamma_{\text{side}}) & \sin(\gamma_{\text{side}})\sin(\gamma_i) \\ \cos(\gamma_n)\sin(\gamma_{\text{side}}) & \cos(\gamma_i)\cos(\gamma_{\text{side}}) & -\sin(\gamma_i)\cos(\gamma_{\text{side}}) \\ -\sin(\gamma_n) & \sin(\gamma_i) & \cos(\gamma_i) \end{bmatrix}.$$

The tool rotation causes the machining forces (F_{q_1} , F_{q_2} , F_{q_3}) on each tooth to rotate relative to the stationary global coordinate frame (x , y , z) resulting in time-varying cutting forces as follows [22],

$$\begin{Bmatrix} F_x \\ F_y \\ F_z \end{Bmatrix} = \begin{bmatrix} 1 & 0 & 0 \\ 0 & \cos\omega t & -\sin\omega t \\ 0 & \sin\omega t & \cos\omega t \end{bmatrix} \begin{Bmatrix} F_{q_1} \\ F_{q_2} \\ F_{q_3} \end{Bmatrix} \tag{2}$$

where ω is the rotational speed of the boring bar.

In the majority of the boring operations, the radial depth of cut a_p is higher than the nose radius, and the uncut chip area configuration for such a case is shown in Fig. 2(c). This is an especially representative case for roughing operations, where the straight edge of the insert dominates over the nose radius in terms of both the direction and magnitude of the cutting force [19]. The direction of the cutting force tends to approach the side cutting edge angle, γ_{side} , of the insert as shown in Fig. 2(c) [17]. Modal parameters offer insight into the dynamic behavior of a structure in relation to its surface normal such as x, y, and z. Nevertheless, if the side cutting edge angle and the other tool angles are not zero or not negligible it serves as a directional orientation factor and modifies the contribution of the modes means only a fraction of the cutting forces f_f, f_t and f_r results in vibration along x, y and z directions of the boring bar [23]. Therefore, it is important to consider tool angles in the cutting force notation.

A multi-dimensional approach is adopted to model uncut chip area with two-dimensional trapezoidal elements as shown in the Fig. 2(d) similar to the studies of Budak et al. [19] and Wang et al. [22]. Each element is defined by its height, side edge length,

angular orientation, and instantaneous chip thickness b_e, b_i, θ_i and $h_i(t)$ respectively, as seen in the Fig. 2(d). The variation of instantaneous chip thickness can be written as follows [22],

$$\Delta h_i(t)(\sin^2(\theta_i) + \cos^2(\theta_i)) = \Delta q_1(t)\sin(\theta_i) + \Delta q_2(t)\cos(\theta_i) \tag{3}$$

$$\Delta h_i(t) = \Delta q_1(t)\sin\theta_i + \Delta q_2(t)\cos\theta_i \tag{4}$$

Δq_1 and Δq_2 denote the relative dynamic displacements between the cutting insert and workpiece in the q_1 and q_2 directions, respectively as shown in Fig. 2(d). They are computed as the difference between the current and previous states of their relative positions at the same angular position along the spiral cutting path of boring. Only dynamic displacements are considered because they are the sole contributors to the dynamic chip load regeneration mechanism. The stiffness of the boring bar in the axial direction (feed direction (x)) is very high; thus, the relative dynamic displacement of the system in the axial direction can be neglected. The total variation of the uncut chip area can be expressed as the sum of the changes in the area of each single element as follows [22],

$$\begin{aligned}
&\Delta A_i(t) = b_i \Delta h_i(t) = \frac{b_e}{\cos\theta_i}(\Delta q_1(t)\sin\theta_i + \Delta q_2(t)\cos\theta_i)\\
&\Delta A_i(t) \approx b_e \Delta q_2(t)\\
&\Delta A \approx \left(\sum_{i=1}^{n} b_{e,i}\right)\Delta q_2(t)
\end{aligned} \tag{5}$$

where n is the total number of trapezoidal elements in the uncut chip area. For cutting inserts with a small radius, it is reasonable to assume that the sum of the heights of the elements b_e in the cutting area equals the radial depth of the cut as follows, $\sum_{i=1}^{n} b_e \approx a_p$. Therefore, the total variation of the uncut chip area can be assumed as,

$$\Delta A(t) \approx a_p\ \Delta q_2(t)\ . \tag{6}$$

Regenerative forces in feed, radial, and tangential directions of the cutting insert that contribute to the regeneration mechanism are found as a product of specific cutting pressures and the total variation in the uncut chip area $\Delta A(t)$ as follows,

$$\begin{cases}
F_f(t) = K_f\ \Delta A(t)\\
F_r(t) = K_r\ \Delta A(t)\\
F_t(t) = K_t\ \Delta A(t)
\end{cases} \tag{7}$$

where K_f, K_r, and K_t, are the specific cutting pressures in feed, radial and tangential directions respectively. By summing the cutting forces contributed by all inserts (m : number of inserts), it is possible to write the total dynamic boring forces acting on the boring bar in radial and tangential vibration directions of the boring bar (y and z respectively) as follows,

$$F_{y,z} = \sum_{i=0}^{m-1} F_{y_i,z_i}(\omega t + m\varphi_{pitch}) \tag{8}$$

where φ_{pitch} is the pitch angle between inserts. To derive the overall cutting force equation, Eq. (7) is substituted into Eq. (1), and then, the resulting expression is plugged into Eq. (2). By summing up all the contributions from the inserts mentioned in Eq. (8) and rearranging the equations, it is possible to arrive at the following expression,

$$\begin{Bmatrix} F_y \\ F_z \end{Bmatrix} = \frac{1}{2} a_p K_t \begin{bmatrix} \alpha_{yy} & \alpha_{yz} \\ \alpha_{zy} & \alpha_{zz} \end{bmatrix} \begin{Bmatrix} \Delta y \\ \Delta z \end{Bmatrix} \tag{9}$$

$$F(t) = \frac{1}{2} a_p K_t [A_D]\{\mathbf{q}(t) - \mathbf{q}(t-\tau)\} \tag{10}$$

where the displacement vector is $\mathbf{q}(\mathbf{t})$ in two orthogonal directions y and z. The directional coefficient matrix $A_D(t)$ is periodically time-varying at $T = \frac{2\pi}{\omega}$, unlike traditional boring or turning operations with a stationary bar. The time-varying directional boring force coefficients are found as follows [22],

$$\begin{cases}
\alpha_{yy} = \sum_{i=0}^{m-1} \beta_1 (1 + \cos(2\omega t)) + \beta_2 \sin(2\omega t)\\
\alpha_{yz} = \sum_{i=0}^{m-1} -\beta_1 \sin(2\omega t) + \beta_2 (1 + \cos(2\omega t))\\
\alpha_{zy} = \sum_{i=0}^{m-1} -\beta_1 \sin(2\omega t) - \beta_2 (1 - \cos(2\omega t))\\
\alpha_{zz} = \sum_{i=0}^{m-1} \beta_1 (1 - \cos(2\omega t)) + \beta_2 \sin(2\omega t)
\end{cases}$$

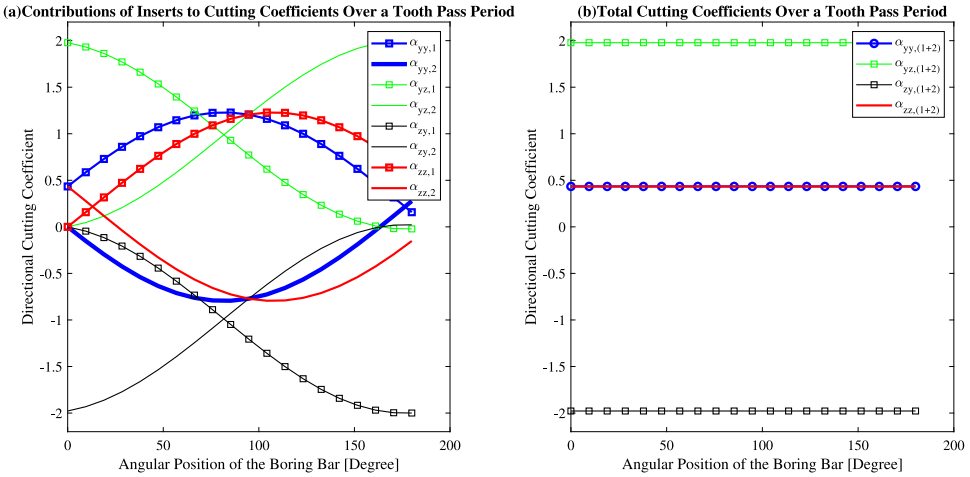

Fig. 3. Directional cutting coefficients.

where

$$\begin{cases} \beta_1 = \cos(\gamma_n) \cdot \sin(\gamma_{\text{side}}) \frac{K_f}{K_t} + \cos(\gamma_i) \cos(\gamma_{\text{side}}) \frac{K_r}{K_t} - \sin(\gamma_i) \cos(\gamma_{\text{side}}) \frac{K_t}{K_t} \\ \beta_2 = -\sin(\gamma_n) \frac{K_f}{K_t} + \sin(\gamma_i) \frac{K_r}{K_t} + \cos(\gamma_i) \frac{K_t}{K_t} \end{cases}$$

Since the directional coefficient matrix $[A_D]$ is a periodic function, it can be expressed as follows by Fourier Series,

$$[A_D(t)] = \sum_{n=-\infty}^{+\infty} [\Lambda_n] e^{jn\omega t} \quad n = 0, \pm 1, \pm 2, \ldots \tag{11}$$

where ω, T, n and Λ_n are fundamental frequency, period, number of harmonics and the Fourier coefficients, respectively.

The cutting inserts used in the boring head are placed with an angular symmetry, which results in their contributions to the cutting force coefficients having a phase difference of 180°. This means that the dynamic parts of the cutting force coefficients generated by the first insert cancel out those generated by the second insert, as depicted in the Fig. 3(a) (b). (*i.e.* $\alpha_{yy,(1+2)} = \alpha_{yy,1} + \alpha_{yy,2}$) .This phenomenon could be compared to the use of the zero-order approximation [24], in which only the average term in the Fourier Series expansion is taken into account. However, in the case of insert run-outs, the uncut chip area may take on an irregular shape at each tool position, resulting in different contributions from each cutting insert to the cutting force [16]. Despite this, it is still reasonable to adopt zero-order-approximation, because the spindle frequency used in boring operations is generally low, and the natural frequency of the machine tool structure is relatively high, making it unlikely that the harmonics of the directional coefficient matrix will excite the natural modes of the machine tool [16]. Additionally, the higher harmonics of the cutting force are typically low-pass filtered within the dynamic cutting process [25].

The average of the periodic directional cutting coefficients (zero-order Fourier coefficient) is expressed as follows [25],

$$[\Lambda_0] = \frac{1}{T} \sum_{j=0}^{m-1} \int_0^T [A_D(t)]\, dt \tag{12}$$

As a result, the overall dynamic force equation of the boring process (Eq. (10)) can be re-written as follows,

$$F(t) = \frac{1}{2} a_p K_t [\Lambda_0] \{\mathbf{q}(t) - \mathbf{q}(t-\tau)\} \tag{13}$$

where $\Lambda_0 = \begin{bmatrix} \alpha_{yy,0} & \alpha_{yz,0} \\ \alpha_{zy,0} & \alpha_{zz,0} \end{bmatrix}$ is the average directional coefficient matrix.

2.1.2. Dynamics of boring process with stiffness variation

Compared to the rigid machine tool bed and workpiece, the boring bar has relatively low radial and tangential stiffness in y and z respectively as seen in Fig. 4. However, it is considerably stiffer in the axial direction (x-axis), while flexibility in the radial and tangential directions causes chatter vibrations. Besides, boring bars are stiffer in torsion around the x-axis as seen in Fig. 4 than in bending along radial and tangential directions [26]. Therefore, the dynamic model of the boring bar was assumed to be a two-degrees-of-freedom lumped mass–spring-damper system as can be seen in Fig. 4 in the radial and tangential directions whose effective stiffness and mass are defined at the point of attachment of the cutting insert and the workpiece. Additionally, chatter generally occurs at the boring bar's lowest natural frequency, resulting in a single dominant vibration mode in each of the two orthogonal axes of the tool [27].

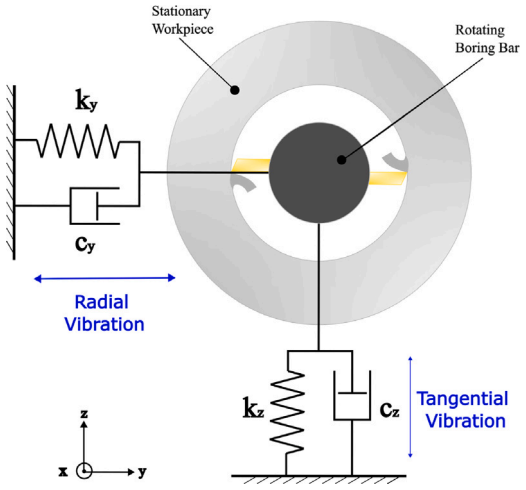

Fig. 4. Lumped spring mass damper model.

The generic form of the equation of motion can be written as follows,

$$\mathbf{M}\ddot{\mathbf{q}}(t) + \mathbf{C}\dot{\mathbf{q}}(t) + \mathbf{K}(t)\mathbf{q}(t) = \mathbf{F}(t) \tag{14}$$

M, **C**, and **K** are mass, damping, and stiffness matrices respectively while $\mathbf{q}(t)$ is a position vector in two orthogonal directions. For the sake of simplicity, it was assumed that only the stiffness of the system is considered as time periodic $K(t) = K(t+T)$ as in [28].

The cutting insert passes over a surface that has already been machined and marked with vibrations from previous rotations. The cutting force fluctuates based on the interaction between the current and previous tool positions at the same angular position of the hole circumference. Structural dynamics influence the cutting process through tool vibrations and cutting forces, resulting in a regenerative chatter phenomenon. The concept of SV is to disturb this regenerative mechanism by modulating the stiffness around its nominal value and causing the natural frequency to change, thus, the machining process alternates between stable and unstable conditions and effectively suppresses chatter. In unstable cutting conditions, the cutter vibrates at chatter frequency ω_c which is very close to the natural frequency of the structure. Changing the natural frequency of the system by altering its stiffness can stabilize the cutting process and suppress chatter. However, if the structural stiffness remains constant, the vibration frequency may shift to a new unstable frequency during cutting [10]. Therefore, continuous change in the natural frequency should be chosen for chatter suppression [8]. The most common signals used for SV are sine, square, and triangle waves. Since a sinusoidal signal is easier for mechanical systems to track and easier for computer numerical control (CNC) realization, the stiffness is assumed to vary in the form of a sinusoidal wave and the modal stiffness of the boring process has the form as follows [28],

$$k_{y,z}(t) = \omega_{ny,z}^2\left(1 + f_{y,z}(t)\right) = \omega_{ny,z}^2\left(1 + a_{sv}\sin\left(2\pi f_{sv}t\right)\right) \tag{15}$$

where a_{sv} is the amplitude ratio and f_{sv} is the frequency of the sinusoidal SV function. By assuming SV in two orthogonal directions and combining the Eqs. (13) and (14), the final equation of motion can be written as follows,

$$\begin{aligned}&\ddot{\mathbf{q}}(t) + \begin{bmatrix} 2\zeta_y\omega_{ny} & 0 \\ 0 & 2\zeta_z\omega_{nz}\end{bmatrix}\dot{\mathbf{q}}(t) + \begin{bmatrix}\omega_{ny}^2(1+f_y(t)) & 0 \\ 0 & \omega_{nz}^2(1+f_z(t))\end{bmatrix}\mathbf{q}(t)\\ &= \frac{1}{2}\,a_p\,K_t\begin{bmatrix}1/m_y & 0 \\ 0 & 1/m_z\end{bmatrix}\begin{bmatrix}\alpha_{yy,0} & \alpha_{yz,0} \\ \alpha_{zy,0} & \alpha_{zz,0}\end{bmatrix}\left[\mathbf{q}(t) - \mathbf{q}(t-\tau)\right] = \begin{bmatrix}F_y \\ F_z\end{bmatrix}.\end{aligned} \tag{16}$$

The dynamics of the LTP systems are governed by differential equations with time-varying and periodic coefficients. This periodicity results from the SV control strategy with a period $T_{sv} = \frac{1}{f_{sv}}$. It should be noted that the equation of motion of the system is delayed also since the chip thickness depends on the instantaneous $q(t)$ and past $q(t-\tau)$ positions of the cutting insert. Constant frequency of SV was employed, whereby it remains independent of the spindle speed. Consequently, TPTDR exhibits continuous variation during the computation of the stability lobe diagram. Starting from Eq. (16), the state-space representation of the system which is more convenient to manipulate in the stability analysis is as follows,

$$\begin{aligned}\dot{\mathbf{q}}_s(t) &= \mathbf{A}(t)\mathbf{q}_s(t) + \mathbf{B}(t)\mathbf{u}(t)\\ \mathbf{g}(t) &= \mathbf{C}(t)\mathbf{q}_s(t) + \mathbf{D}(t)\mathbf{u}(t)\end{aligned} \tag{17}$$

Table 1
Input–output characteristics of LTI/LTP systems.

System	Input	Output
LTI	$\mathbf{u}(t) = e^{st}$	$\mathbf{y}(t) = Ae^{st+\phi}$
LTP	$\mathbf{u}(t) = 1 + \sin \omega t$	$\mathbf{y}(t) = e^{st} + e^{(s+i\omega_p)t} + e^{(s-i\omega_p)t}$

Where $s \in \mathbb{C}$.

where

$$[\mathbf{A}] = \begin{bmatrix} 0 & 0 & 1 & 0 \\ 0 & 0 & 0 & 1 \\ -\omega_{ny}^2(1+f_y(t)) & 0 & -\zeta_y\omega_{ny} & 0 \\ 0 & -\omega_{nz}^2(1+f_z(t)) & 0 & -2\zeta_z\omega_{nz} \end{bmatrix} \quad [\mathbf{B}] = \begin{bmatrix} 0 & 0 \\ 0 & 0 \\ \frac{1}{m_y} & 0 \\ 0 & \frac{1}{m_z} \end{bmatrix}$$

$$[\mathbf{C}] = \begin{bmatrix} 1 & 0 & 0 & 0 \\ 0 & 1 & 0 & 0 \end{bmatrix} \quad [\mathbf{D}] = 0 \quad \mathbf{u} = \begin{bmatrix} F_y \\ F_z \end{bmatrix} \quad \text{and} \quad \mathbf{q_s}(t) = \begin{Bmatrix} y \\ z \\ \dot{y} \\ \dot{z} \end{Bmatrix}.$$

A, **B**, **C**, and **D** are dynamics, input, output, and feedthrough matrices respectively. $\mathbf{q_s}$, **u**, and **g** are state, input, and output vectors respectively.

2.2. Stability analysis: Frequency domain representation and harmonic solution

The suppression of chatter can be achieved through the periodic adjustment of system parameters, resulting in the creation of a LTP system. While a sinusoidal input in a LTI system produces a sinusoidal output with a distinct amplitude A and phase ϕ, the output of a LTP system driven by a complex exponential consists of a combination of sinusoids at $\omega + in\omega_p$ where ω_p is typically known as the pumping frequency and n is the integer multiplier for its harmonics as shown in the Table 1. As a consequence, the transfer function method proves to be an unreliable approach for describing the input–output relationship in LTP systems, as noted by Wereley et al. [15].

The stability analysis of LTP systems with HS was originally introduced by Wereley et al. [15]. This method was further developed and generalized as a means of analyzing chatter in milling by Defant et al. [14]. In the present study, the generalized HS approach [14] was adopted and applied to the stability analysis of the boring process. Hereafter, a summary of this approach was provided as it pertains to this specific research.

Due to the LTP dynamics, the state matrix $\mathbf{A}(t)$ is periodic at $T = \frac{1}{f_{sv}}$ so that,

$$\mathbf{A}(t+T) = \mathbf{A}(t) \qquad \forall\ T\ in\ (-\infty, +\infty) \tag{18}$$

To assess the stability of a LTP system, an exponentially modulated periodic (EMP) test signal ($u(t) = \sum_{n=-\infty}^{+\infty} U_n e^{(s+in\omega_p)t}$ where $s \in \mathbb{C}$ and n is the integer multiplier of its harmonics) is utilized as the input which ensures that also the output signal exhibits periodic behavior.

Therefore, the state matrix $\mathbf{A}(t)$, input vector $\mathbf{u}(t)$, and output vector $\mathbf{g}(t)$ can be expressed in terms of complex Fourier series. By substituting these expressions into Eq. (17), the state space representation can be obtained using harmonic balance [15],

$$\begin{aligned} sq_s &= (\mathcal{A} - \mathcal{N})q_s + \mathcal{B}u \\ g &= Cq_s + \mathcal{D}u \end{aligned} \tag{19}$$

where $\mathcal{N} = blk\{in\omega_p I\}$ is a block diagonal matrix containing all harmonics of the pumping frequency. In this notation, q_s, u, and g are state, control, and output vectors at different harmonics, respectively. $\mathcal{A}, \mathcal{B}, \mathcal{C}, \mathcal{D}$ matrices are in block-Toeplitz form due to the Toeplitz transformation as described in detail in the study of Wereley et al. [15]. This transformation takes the group of complex Fourier coefficients and maps it to a doubly infinite block Toeplitz matrix and makes it possible to transform time-periodic ordinary differential equations into infinite-dimensional algebraic equations that are time-invariant.

Harmonic transfer function $\mathbf{H}(s)$ is an infinite dimensional matrix that describes the input and output relationship between the harmonics of the input and output signal as follows [15],

$$\begin{aligned} \mathbf{H}(s) &= C\left[sI - \left(\mathcal{A} - \mathcal{N}\right)\right]^{-1}\mathcal{B} + \mathcal{D} \\ Y &= \mathbf{H}(s)\ U. \end{aligned} \tag{20}$$

The harmonic transfer function $\mathbf{H}(s)$ in LTP systems is analogous to the transfer function of LTI systems. To better understand the dimensions of the matrices, Eq. (20) can be written as follows in Eq. (21) in matrix notation with impulse response

representation [14],

$$\begin{pmatrix} \vdots \\ \mathbf{Y}_{-1} \\ \mathbf{Y}_0 \\ \mathbf{Y}_1 \\ \vdots \end{pmatrix} = \begin{bmatrix} \ddots & \vdots & \vdots & \vdots & \iddots \\ \dots & \mathbf{H}_0(s-i\omega_p) & \mathbf{H}_{-1}(s) & \mathbf{H}_{-2}(s+i\omega_p) & \dots \\ \dots & \mathbf{H}_1(s-i\omega_p) & \mathbf{H}_0(s) & \mathbf{H}_{-1}(s+i\omega_p) & \dots \\ \dots & \mathbf{H}_2(s-i\omega_p) & \mathbf{H}_1(s) & \mathbf{H}_0(s+i\omega_p) & \dots \\ \iddots & \vdots & \vdots & \vdots & \ddots \end{bmatrix} \begin{pmatrix} \vdots \\ \mathbf{U}_{-1} \\ \mathbf{U}_0 \\ \mathbf{U}_1 \\ \vdots \end{pmatrix} \tag{21}$$

The harmonic transfer function's main diagonal links same-frequency input and output harmonics, reflecting the LTI system. In contrast, the off-diagonal terms connect different frequency harmonics and are critical for assessing stability in LTP systems. For the numerical implementation of the described procedure in computer, truncation is needed while ensuring adequate representation of the system dynamics. As more harmonics are considered, the matrices become larger, creating a trade-off between modeling accuracy and computational effort. For instance, the dimension of the system matrix $\mathcal{A}$ has 12 rows and columns if only a single harmonic is considered. On the other hand, if the number of harmonics is increased to 5, then the system matrix $\mathcal{A}$ will have dimensions of 44×44 which increases computational effort.

Considering EMP signal for the force $F(t)$ and the variation at the state $\mathbf{q_s}(t) - \mathbf{q_s}(t-\tau)$ as follows as a Fourier Series [14],

$$\begin{aligned} F(t) &= \sum_{n=-\infty}^{+\infty} \mathbf{P}_n e^{s_n t} \qquad \text{where} \quad s_n = s + in\omega_p \quad \text{and} \quad n \in \mathbb{Z} \\ \mathbf{q_s}(t) - \mathbf{q_s}(t-\tau) &= \sum_{m=-\infty}^{+\infty} \mathbf{Q}_m e^{s_m t} \ (1 - e^{-s_m \tau}) \qquad \text{where} \quad s_m = s + im\omega_p \quad \text{and} \quad m \in \mathbb{Z}. \end{aligned} \tag{22}$$

where $\mathbf{P}_n$ and $\mathbf{Q_m}$ are the Fourier coefficients of force and state signal respectively. Rewriting the state Fourier coefficients $\mathbf{Q}_m$ in terms of the harmonic transfer function $\mathbf{H}$ and Fourier coefficients $\mathbf{P}_n$ of the input signal with impulse response representation as follows [29],

$$\mathbf{Q}_m = \sum_{n=-\infty}^{+\infty} \mathbf{H}_{n-m}(s - in\omega_p)\mathbf{P}_n \tag{23}$$

Substituting the Eqs. (11), (22) and (23) into cutting force Eq. (13) and rearranging the equations in Toeplitz notation leads to Eq. (24) as described in detail in the study of Defant et al. [14].

$$\mathbf{P} = \frac{1}{2} a_p K_t \left(\Lambda' - \Lambda'\varepsilon\right) \mathcal{H}\ \mathbf{P} \qquad \text{where} \qquad \varepsilon = I e^{-i(\omega_c + m\omega_p)\tau}. \tag{24}$$

where Λ' denotes for time-varying directional cutting force coefficient matrix including all harmonics. As previously shown, the zero-order approach is adopted in the time-varying directional cutting force coefficient matrix to have Λ_0 and it is scaled to achieve matrix Λ_0' compatible with $n \geq 1$.

$$\Lambda_0' = \begin{bmatrix} [\Lambda_0] & \dots & [0] \\ \vdots & [\Lambda_0] & \vdots \\ [0] & \dots & [\Lambda_0] \end{bmatrix} \tag{25}$$

It should be noted that the extra-diagonal terms of the directional cutting force coefficient matrix Λ_0 are zero. Furthermore, the pumping frequency is equal to the SV frequency ($\omega_p = \omega_{sv}$), thus, the zero-order harmonic solution (ZOHS) can be written by extending the matrices as follows [14],

$$\begin{aligned} \begin{pmatrix} \vdots \\ \mathbf{P}_{-1} \\ \mathbf{P}_0 \\ \mathbf{P}_1 \\ \vdots \end{pmatrix} = \frac{1}{2}\ a_p\ K_t \left(\begin{bmatrix} \ddots & \vdots & \vdots & \vdots & \iddots \\ \dots & \mathbf{I} & 0 & 0 & \dots \\ \dots & 0 & \mathbf{I} & 0 & \dots \\ \dots & 0 & 0 & \mathbf{I} & \dots \\ \iddots & \vdots & \vdots & \vdots & \ddots \end{bmatrix} - \begin{bmatrix} \ddots & \vdots & \vdots & \vdots & \iddots \\ \dots & e^{-i(\omega_c - \omega_{sv})\tau} & 0 & 0 & \dots \\ \dots & 0 & e^{-i\omega_c \tau} & 0 & \dots \\ \dots & 0 & 0 & e^{-i(\omega_c + \omega_{sv})\tau} & \dots \\ \iddots & \vdots & \vdots & \vdots & \ddots \end{bmatrix} \right) \\ \begin{bmatrix} \ddots & \vdots & \vdots & \vdots & \iddots \\ \dots & \Lambda_0 & 0 & 0 & \dots \\ \dots & 0 & \Lambda_0 & 0 & \dots \\ \dots & 0 & 0 & \Lambda_0 & \dots \\ \iddots & \vdots & \vdots & \vdots & \ddots \end{bmatrix} \begin{bmatrix} \ddots & \vdots & \vdots & \vdots & \iddots \\ \dots & \mathbf{H}_0(s - i\omega_{sv}) & \mathbf{H}_{-1}(s) & \mathbf{H}_{-2}(s + i\omega_{sv}) & \dots \\ \dots & \mathbf{H}_1(s - i\omega_{sv}) & \mathbf{H}_0(s) & \mathbf{H}_{-1}(s + i\omega_{sv}) & \dots \\ \dots & \mathbf{H}_2(s - i\omega_{sv}) & \mathbf{H}_1(s) & \mathbf{H}_0(s + i\omega_{sv}) & \dots \\ \iddots & \vdots & \vdots & \vdots & \ddots \end{bmatrix} \begin{pmatrix} \vdots \\ \mathbf{P}_{-1} \\ \mathbf{P}_0 \\ \mathbf{P}_1 \\ \vdots \end{pmatrix} \end{aligned} \tag{26}$$

For an LTI system, the extra-diagonal terms of the harmonic transfer function $H(i\omega_c)$ will be zero, and only diagonal terms that correspond to frequency response functions will be left. Therefore, the solution for the LTI system can be written as follows,

$$\mathbf{P}_0 = \frac{1}{2} a_p K_t \left(1 - e^{-i\omega_c \tau}\right) \Lambda_0 \mathbf{H}_0(i\omega_c)\mathbf{P}_0 \tag{27}$$

To draw a stability lobe diagram, the roots of the characteristic Eq. (27) must be found by solving the determinant below,

$$det\left(I - \frac{1}{2} a_p K_t (\Lambda_0 - \Lambda_0 \varepsilon)\mathbf{H_0}\right) = 0 \tag{28}$$

To solve the root-finding problem, a two-equation system is utilized for the transfer function's real and imaginary parts, along with three variables (depth of cut, spindle speed, and chatter frequency). Stable depth of cut is defined for various chatter frequencies

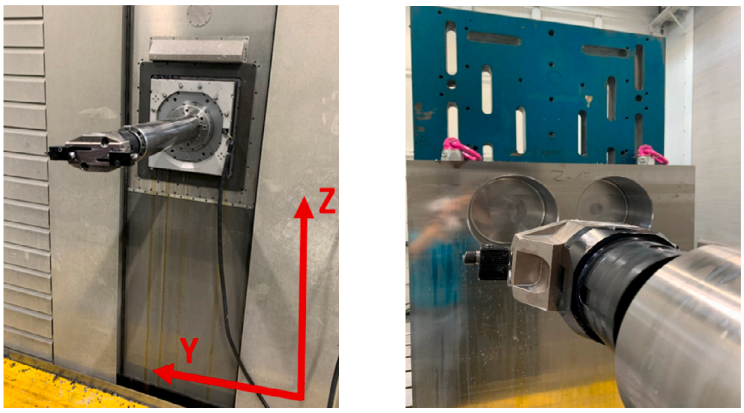

Fig. 5. Rotating boring bar with two inserts (a) and example workpiece (b).

around the most flexible structural mode, and spindle speeds are identified for different lobes. The stability diagram is created by plotting the stable depth of cut against spindle speeds for different lobes [25].

The bisection method is a root-finding algorithm for any continuous non-linear function if two values of the function with opposite signs are known. It involves iteratively bisecting an interval and checking the sign of the midpoint to locate the root. Bachrathy et al. [30] extended the one-dimensional intersection problem into multiple dimensions to find multiple roots. In this study, this method is employed to solve a stability problem. Node data in the 3-dimensional n-cube is stored in arrays (using MATLAB in this research), and neighboring object coordinates are determined with predefined initial mesh size and boundary values for each dimension, including the depth of cut, spindle speed, and chatter frequency. The final step of the algorithm involves interpolating the roots inside the bracketing n-cubes. The result is a point cloud representing the stability boundary surface in three dimensions: $depth of cut, spindle speed, and chatter frequency.$

3. Results and discussion

Firstly, the experimental setup was described, encompassing modal parameters, workpiece material properties, and cutting tool geometry. Thereafter, experimental validation of the proposed dynamical model and stability analysis method for a multi-insert rotating boring bar was conducted in the absence of any SV application (Validation 1, see Fig. 1). Furthermore, to show the comprehensiveness of the proposed model, a second validation activity has been performed by comparing the estimated stability lobe diagrams with the experimental data obtained from other studies in the literature for the case of single-insert stationary boring bars encompassing cases with and without SV (Validation 2, see Fig. 1). In this way, the capability of the generalized harmonics solution to accurately predict stability lobe diagrams of LTP systems in boring applications was demonstrated. In addition, for the application of a generalized HS in stability analysis, the minimum number of harmonics needed to adequately represent the boring dynamics with time-varying parameters was determined by performing convergence analysis. Moreover, a sensitivity analysis was conducted to investigate the effect of SV amplitude and frequency on the chatter suppression performance for both single-insert stationary boring bars and multiple-insert rotating boring bars. Lastly, the sensitivity analysis results of single-insert stationary boring bars were validated by comparing them with experimental data taken from other studies in the literature(Validation 3, see Fig. 1).

3.1. Description of the experimental setup

The apparatus employed for experimental validation is a precision boring machine featuring a rotating boring bar equipped with multiple inserts. The boring bar advances linearly toward the workpiece at a predetermined feed rate. Meanwhile, the workpiece is securely fastened to a stationary table, as illustrated in Fig. 5.

The large-scale boring machine tool consists of a machining carriage supporting a movable ram, which can move relative to the carriage in the feed direction which can be seen in Fig. 6. A boring bar, supported by the ram, is also movable along the feed direction with respect to the ram. The cutting head is rotated by a spindle, which is supported by the boring bar. This machine possesses the capability to adjust its stiffness by interpolating displacements of the ram and boring bar along two parallel axes of the machine tool as detailed in patent number WO 2021/009617. During machining, the ram and the boring bar move in opposite directions, covering equal distances, thereby maintaining the position of the tool unchanged. The waveform of the continuous periodic stiffness variation is sinusoidal. The SV frequency ranges from 1 to 5 Hz, with an SV amplitude of up to 30%, while ensuring simultaneous positioning of axes. With pressure control, the SV frequency can be increased to up to 50 Hz, with an SV amplitude ranging from 5 to 10%.

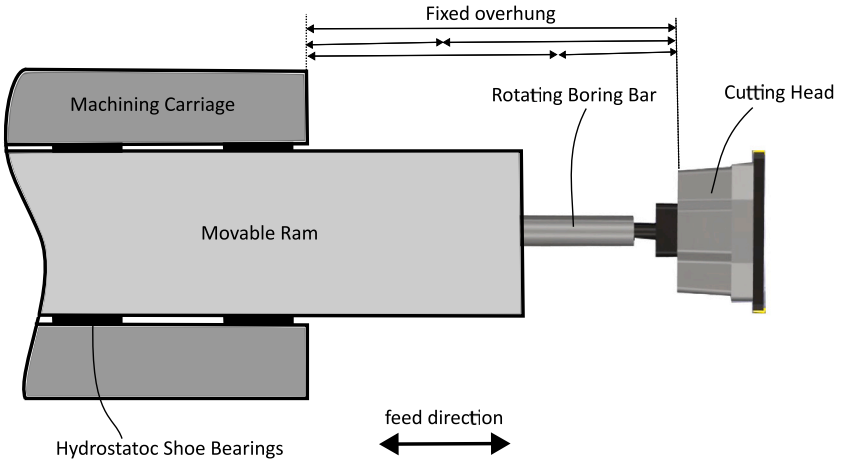

Fig. 6. Boring machine schematic drawing.

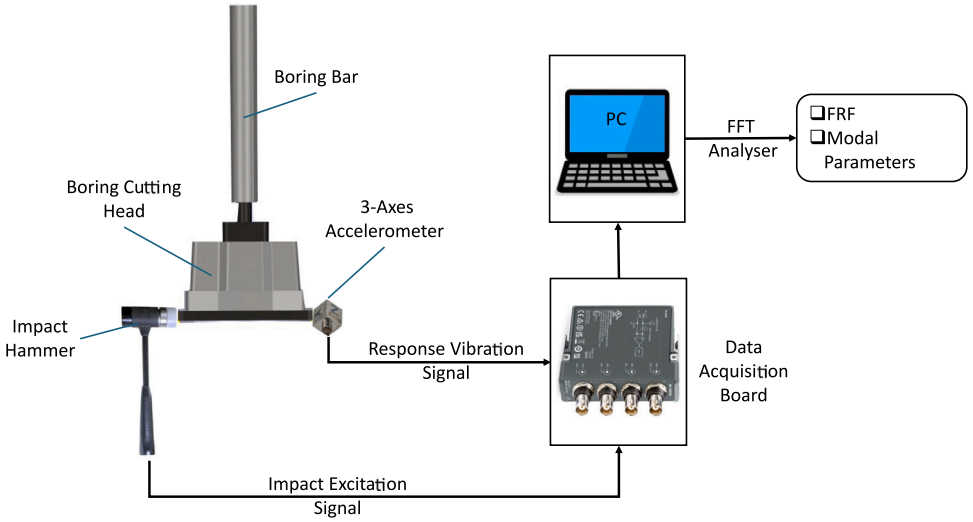

Fig. 7. Experimental setup for modal testing.

To construct a stability lobe diagram, it is essential to have a thorough understanding of the frequency response function of the cutting head-boring bar-machine system, particularly as observed at the tool point. The experimental platform utilized for modal testing incorporates essential instrumentation components for dynamic characterization and cutting test monitoring. These instruments include the instrumented hammer PCB 086D20 for system excitation, the triaxial accelerometer (PCB 356A32) for dynamic characterization during impact hammer tests, and the triaxial accelerometer (DYTRAN 321M6) for monitoring cutting tests, acquiring acceleration signals under different cutting conditions. All data are collected by the acquisition board (National Instruments NI 9234). The specifications of instruments used in the experimental activities are summarized in Table 2. During modal testing as depicted in Fig. 7, the boring bar undergoes impacts at the cutting inserts' location using the impact hammer. The accelerometers attached to the cutting inserts capture the structure's response, and the resulting signals are analyzed using a dynamic signal analyzer. Coherence plots validate the transfer function, ensuring that observed peaks correspond to resonant frequencies of the boring bar structure. Frequency response functions are computed using the fast fourier transform algorithm. Modal parameter identification entails a blend of the half-power method and circle fit techniques, customized for multi-degree-of-freedom systems, ensuring robust characterization of structural dynamics.

The modal parameters, including natural frequency (ω_n), modal stiffness (k), and damping ratio (ζ), obtained through impact hammer testing, are presented in Table 3.

The specific cutting pressures and tool angles employed in the analytical formulation are detailed in Table 4.

Table 2
Instruments used in the experimental activities.

Instrument	Specifications
Instrumented hammer PCB 086D20	Mass 1.1 kg, sensitivity 0.23 mV/N, measurement range ±22 240 N
Triaxial accelerometer PCB 356A32	Sensitivity 100 mV/g, measurement range ±50 g, frequency range 1÷4000 Hz (5%)
Triaxial accelerometer Dytran 321M6	Sensitivity 100 mV/g, range ±50 g, frequency range 1.5÷5000 Hz (10%)
Acquisition board NI 9234	NI ENET-9163 case

Table 3
Modal parameters.

Direction	ω_n [Hz]	k [N/m]	ζ
Y	99.5	4 460 000	8.48%
Z	100	14 950 000	2.61%

Table 4
Material and insert data.

Material data	Tangential specific cutting pressure K_t	1500 N/mm^2
	Radial specific cutting pressure Kr	$K_t/4$
	Feed specific cutting pressure K_f	$K_t/3$
Insert angles	Normal rake angle γ_n	5°
	Side cutting-edge angle γ_{side}	30°
	Inclination angle γ_i	5°

3.2. Experimental validation

3.2.1. Model validation of multi-insert rotating boring bar

In this section, the experimental validation of the multi-insert rotating boring bar model without SV was presented. The stability lobe diagram (SLD) for the boring machine tool, as discussed in Section 3.1, was computed using the modal parameters, material data, and cutting insert geometry reported in Tables 3 and 4.

The experimental validation was conducted at six different operating points, with a 3 mm radial depth of cut and varying spindle speeds which are 120,130,140,150,160 and 170 rpm as shown in Fig. 10. The resulting SLD indicates an asymptotic stability limit of approximately 0.28 mm in the radial direction, for spindle speeds ranging from 100 rpm to 200 rpm.

In Fig. 8, the cutting surfaces corresponding to all experimental points are displayed, covering rotational speeds ranging from 120 to 170 rpm, with a depth of cut set at 0.3 mm. Additionally, Fig. 9 showcases the cutting acceleration signals along with their frequency content for each experimental point. These visuals provide insights into the cutting conditions. At a spindle speed of 120 rpm, vibration was observed, indicating the system transitioning between stable and unstable states, as evidenced by the vibration acceleration signal. At spindle speeds of 130, 140, and 150 rpm, chatter vibration occurred around 112 Hz. Conversely, at spindle speeds of 160 and 170 rpm, machining remained stable without excessive vibration.

The analytical results closely align with the experimental findings, exhibiting a remarkable coherence across the majority of data points. In more detail, the operating points at spindle speeds of 130 rpm and 140 rpm are in the unstable region of the SLD. Furthermore, the operating points at 160 rpm and 170 rpm are in the conditional stability region of the SLD. The point in 120 rpm was observed as marginally stable in the experiment as it is also in this condition in the analytical result. However, an exception arises at the operating point of 150 rpm, where analytical predictions demonstrate marginal stability, contrasting with the observed instability in the experimental setup. Bistability in machining, as evidenced by the stability lobe diagram, indicates that the process can either proceed smoothly or exhibit chatter depending on specific parameters, highlighting the complexity of machining dynamics. Discrepancies between anticipated and observed outcomes often stem from uncertainties in dynamic behaviors and operational variables, challenging the accurate prediction of stability lobe diagrams and emphasizing the need for ongoing refinement of stability models [31,32]. It is significant to note that boring applications are generally low-speed processes in which the stability pockets can be very narrow and difficult to distinguish from each other. Therefore, precisely predicting the stability pockets is a difficult task, and the general approach in the literature is to find an asymptotic stability limit instead of drawing stability pockets precisely. In summary, the proposed dynamical model of a multi-insert rotating boring bar has been validated experimentally for the case with LTI dynamic characteristics with a data match of 5 out of 6 operating points.

3.2.2. Model validation of single-insert stationary boring bar

The second validation was conducted on a stationary boring bar equipped with a single insert. This assessment involved a comparison of results with the experimental findings presented in the study of Mei et al. [10], where a MR fluid-controlled boring bar was employed to modulate the stiffness of the boring bar. The referenced study investigated a single insert stationary boring bar across five distinct operating points, characterized by spindle speeds 450, 500, 710, 900, and 1120 rpm, coupled with a 0.2 mm depth of cut. Remarkably, all these operating points exhibited chatter vibration, as indicated by their experimental observations. In this investigation using the same structural and cutting parameters reported in the study of Mei et al. [10], the stability lobe

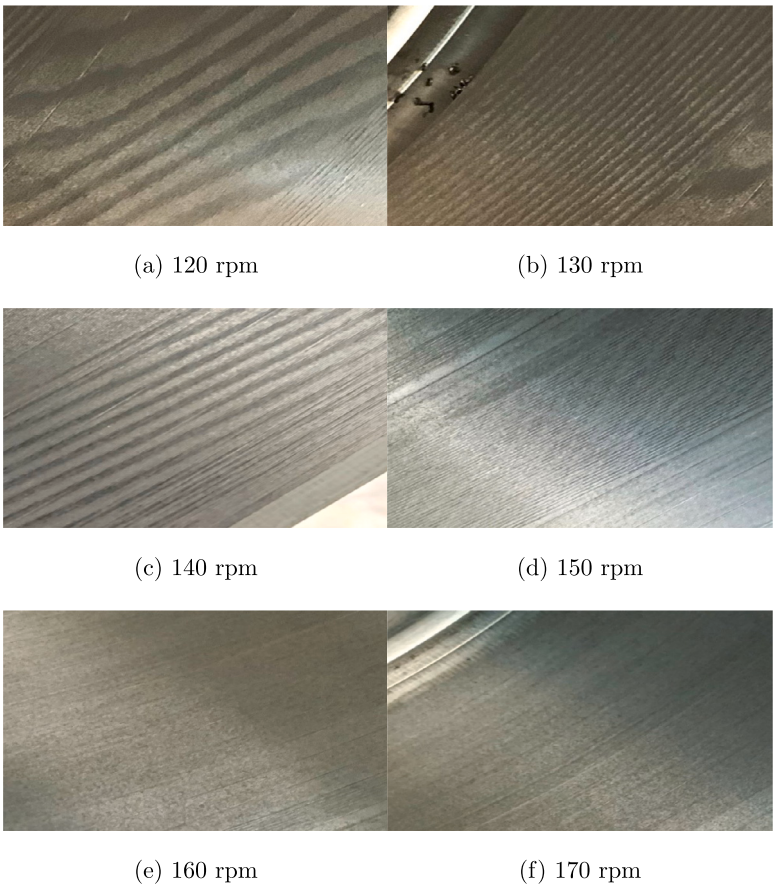

Fig. 8. Cutting surfaces (depth of cut = 0.3 mm).

diagram was found with the proposed analytical methodology as can be seen in Fig. 11. Consistent with the earlier study, all operating points, except for the instance at 900 rpm, were found to be unstable in the stability lobe diagram when SV control was not active. This concurrence reinforces the validity of the proposed boring model for single-insert stationary boring bars, showcasing the comprehensiveness of the proposed model.

To implement the HS computationally, the infinitely dimensional system matrices need to be truncated while ensuring the accurate representation of the system behavior. Convergence analysis has been performed to determine the minimum number of harmonics required for the HS. The analysis reveals that the solution converges to the same stability frontier after incorporating 5 harmonics. Thus, at least 5 harmonics are necessary to precisely perform stability analysis and draw a stability lobe diagram. The stability lobe diagram for the boring process with activated SV (amplitude ratio of 55% and frequency of 1 Hz) is presented in Fig. 11. It is noteworthy that, as reported in [10], all machining processes across the aforementioned operating points transitioned into a chatter-free regime. This alignment is evident also in the analytical stability lobe diagram, where all points reside within the unconditional stability region. The analytical results demonstrate strong agreement with experimental findings, affirming the robustness of the proposed model for stability analysis in systems exhibiting linear-time-periodic dynamics.

The validation of ZOHS was carried out for both a sinusoidal and a piece-wise constant function of SV in the previous work of Defant et al. [14]. Their findings demonstrated close agreement concerning the shape and positioning of stability lobes, as well as the absolute stability limit, as extensively documented in [14]. Overall, the accuracy of ZOHS is almost equivalent to semi-discretization at convergence. However, within the frequency domain, it becomes feasible to disregard higher-order harmonics, thereby markedly reducing computational time. Notably, ZOHS exhibits superior efficiency, enabling the computation of stability lobe diagrams within a timeframe achievable on a standard commercial laptop, surpassing semi-discretization by an order of magnitude [14]. This highlighted computational efficiency results from the truncation of harmonics, focusing solely on those impacting stability. Moreover, the computational effort does not depend on the complexity of the dynamical system, enabling efficient handling of systems featuring multiple critical modes [14]. These attributes address the demands of industrial settings and make the process of SV parameters optimization easier and faster with the utilization of ZOHS. Given the non-trivial nature of the governing dynamics between milling and boring processes, wherein despite the distinct machining operations, the underlying physics and mathematical formulations remain analogous, it can be asserted that ZOHS will exhibit comparable accuracy and a higher efficiency compared to the semi-discretization method.

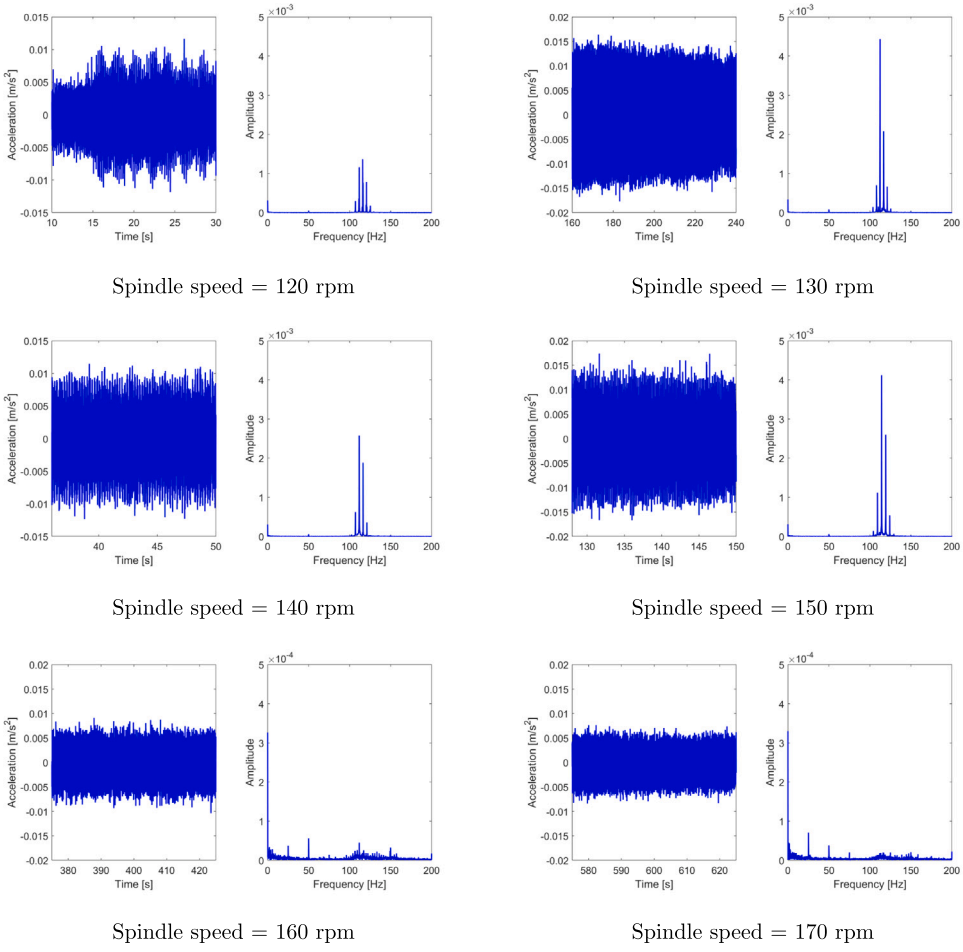

Fig. 9. Vibration acceleration signal of the boring bar (depth of cut = 0.3 mm).

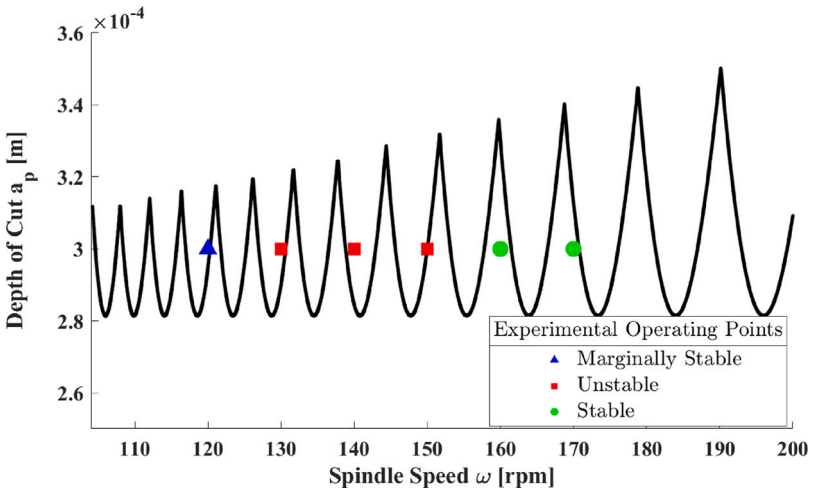

Fig. 10. Stability lobe diagram: Multi-insert rotating boring bar.

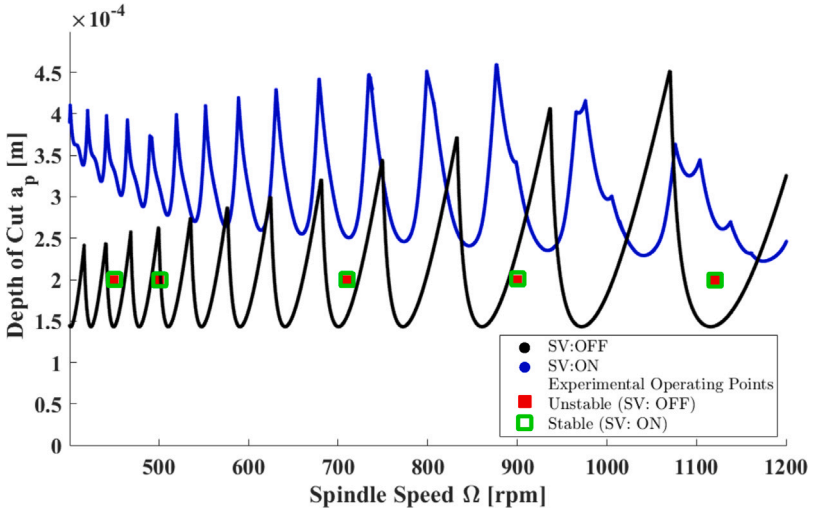

Fig. 11. Stability lobe diagram: Single-insert stationary boring bar.
Source: Experimental data from [10].

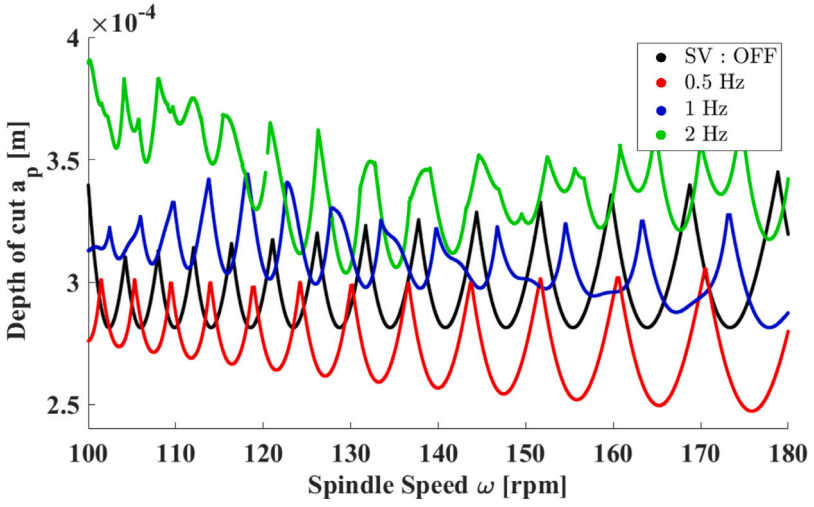

Fig. 12. Sensitivity analysis of stiffness variation frequency (Multi-insert rotating boring bar).

3.3. Sensitivity analysis of stiffness variation parameters

To investigate the effect of SV parameters (amplitude ratio and frequency) on the chatter suppression performance, sensitivity analysis was conducted. The results of the study provide practical insights for selecting optimal SV parameters.

3.3.1. Stiffness variation frequency

In the sensitivity analysis of SV frequency, the same parameters of dynamics, insert geometry, and workpiece material which are reported in Tables 3 and 4 were used considering the multi-insert rotating boring bar model, as discussed in Section 3.1. The amplitude ratio a_{sv} in both radial (y) and tangential (z) axes was set to 20%, and the number of harmonics was set to 5, based on convergence analysis previously performed. As illustrated in Fig. 12, the analytical results indicate that reducing the frequency of SV in both axes, $f_{sv,y}$ and $f_{sv,z}$, from 1 Hz to 0.5 Hz results in a lower asymptotic stability limit than the one of the boring process without SV control. This observation can be attributed to the relatively low SV frequency in relation to the tooth passing frequency. Consequently, the system tends to behave as if in steady-state condition, where stability is governed by instantaneous conditions [33]. However, increasing the frequency to 2 Hz leads to a noticeable improvement in the asymptotic stability limit. The trend of the asymptotic stability limit with changing SV frequency is depicted in Fig. 18.

As it is noticeable in Fig. 12, the stability limit was not improved homogeneously throughout the spindle speed axis in the stability lobe diagram. If the SV frequency is increased to tooth passing frequency (TPF), the chatter suppression might be influenced

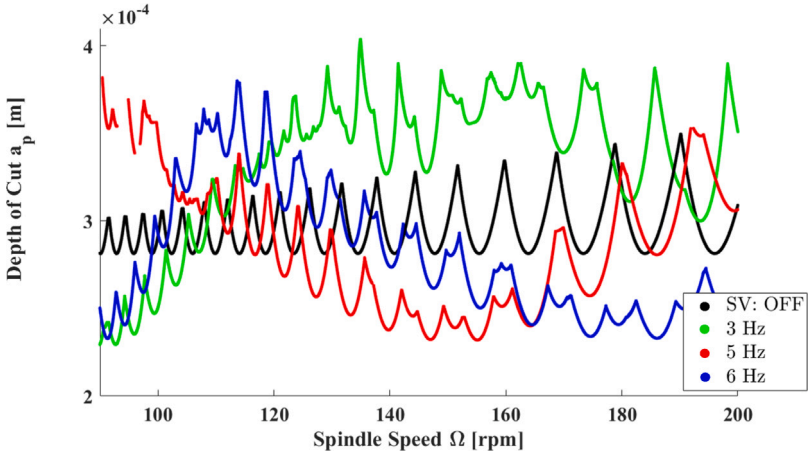

Fig. 13. Sensitivity analysis of stiffness variation frequency (Multi-insert rotating boring bar) (Worst cases).

negatively and this behavior was observed also in [8].

$$TPF[Hz] = \frac{mn}{60} \quad \text{where } m \text{ is the number of inserts, } n \text{ is the spindle speed [rpm]}$$

To better understand this behavior, some example values of 3, 5 and 6 Hz of SV frequencies were applied as expected to have poor performance around 90, 150 and 180 rpm respectively. As shown in Fig. 13, at 3 Hz, there is a noticeable poor performance around 90 rpm. At 5 Hz and 6 Hz, chatter suppression performance decreases around 150 rpm and 180 rpm, respectively. Fig. 18 illustrates the trend of the asymptotic stability limit for varying SV frequency with a 30% amplitude ratio. The presence of a secondary drop around 5 Hz in Fig. 18 is attributed to the plot being applicable to the 130–150 rpm range. Upon aligning the tooth passing frequency with the SV frequency, ineffective chatter suppression was noted, consistent with findings in [8]. This phenomenon is also evident in Fig. 9, particularly around 150 rpm at 5 Hz.

The experimental validation of the sensitivity analysis concerning SV frequency involved a comparison with the findings from Mei et al.'s study [8] on a MR fluid-controlled boring bar. Through modulation of the applied magnetic field strength, the MR fluid exhibits the capability to alter stiffness levels consecutively. Implementing MR fluid around the base of the boring bar enables continuous adjustment of both the bar's stiffness and natural frequency by controlling the intensity of the magnetic field passing through the fluid [8]. The experimental results validate the stability limits across various SV frequency values, thus reinforcing the reliability of the proposed solution in this study. Mei et al. [8] focused on a single-insert stationary boring bar, and the observed patterns in the sensitivity analysis of SV parameters, concerning the effectiveness of chatter suppression, can be extrapolated to multi-insert boring tools. In this study, the structural and workpiece material parameters reported by Mei et al. [8] were employed in the single insert stationary boring bar model. The SV amplitude ratio was set at 40%, with frequencies ranging from 0.2 to 8 Hz. The experiment covered four distinct operating points, with depth of cuts at 0.5, 0.75, 1, and 2 mm, coupled with a spindle speed of 450 rpm. Chatter vibration was consistently observed across all four operating points. However, the implementation of the SV chatter suppression method revealed stabilization effects at 0.5 and 0.8 Hz for a 0.5 mm depth of cut, while instability persisted at 0.2 Hz. This experimental observation aligns with the analytical findings depicted in Fig. 14. At the experimental operating point of (0.5 mm, 450 rpm), instability was identified (represented by a red square). Referring to the findings of [8], instability occurred at a 0.2 Hz SV frequency, while stability was observed at 0.5 Hz and 0.8 Hz. Hence, blue-filled rectangle symbols are used to denote this point, indicating its dependency on SV frequency. This experimental observation aligns with the analytical findings depicted in Fig. 14, where stability lobes of different colors are dedicated to distinct SV frequencies.

Increasing the cutting depth to 0.75 mm revealed experimental results indicating a reduction in vibration accelerations beyond 2 Hz, stabilizing after 4 Hz. Fig. 15 illustrates that these experimental outcomes correspond with the analytical findings presented in this study, where the stability frontier at 1 Hz, 2 Hz, and 4 Hz exceeds the operating point.

Nevertheless, when the depth of cut increased to 2 mm, chatter suppression became unattainable under the given parameters, even at 4, 6, and 8 Hz. This observation is consistent with the analytical findings illustrated in Fig. 16, highlighting the limitation of chatter suppression at higher cutting depths with the specified parameters.

3.3.2. Stiffness variation amplitude

In this section, sensitivity analysis results of SV amplitude a_{sv} from 10% to 40% were presented in Fig. 17. The same parameters of dynamics, insert geometry, and workpiece material which are reported in Tables 3 and 4 were used considering the multi-insert rotating boring bar model which was presented in Section 3.1. SV frequency f_{sv} was set to 3 Hz for both radial (y) and tangential (z) axes, which is approximately the optimal frequency for 140 rpm in terms of stability enhancement. The amplitude ratio was increased up to 40%, which is approximately a limit value that can be implemented in most real-world industrial applications.

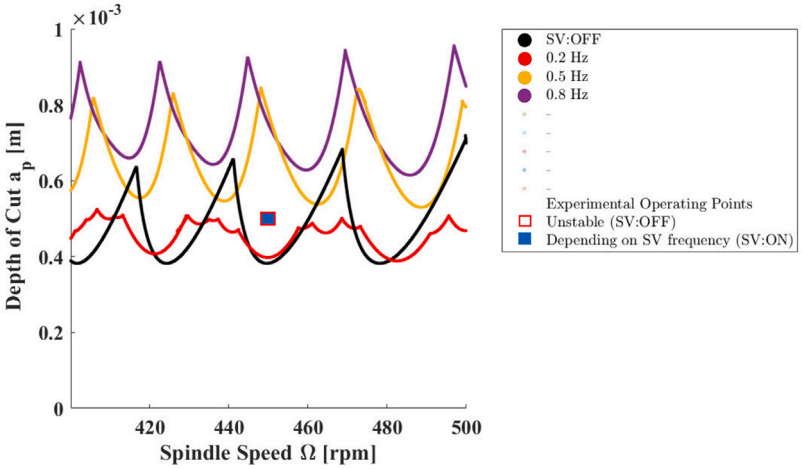

Fig. 14. Sensitivity analysis of stiffness variation frequency (1) (Single-insert stationary boring bar). *Source:* Experimental data from [8].

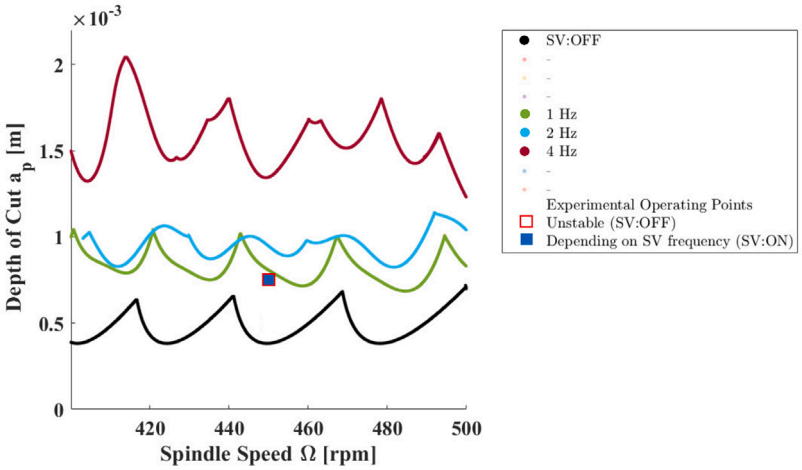

Fig. 15. Sensitivity analysis of stiffness variation frequency (2) (Single-insert stationary boring bar). *Source:* Experimental data from [8]

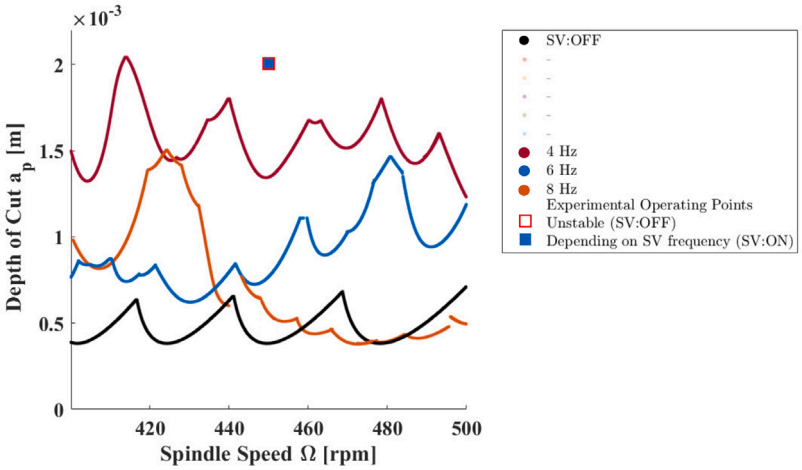

Fig. 16. Sensitivity analysis of stiffness variation frequency (3) (Single-insert stationary boring bar) . *Source:* Experimental data from [8].

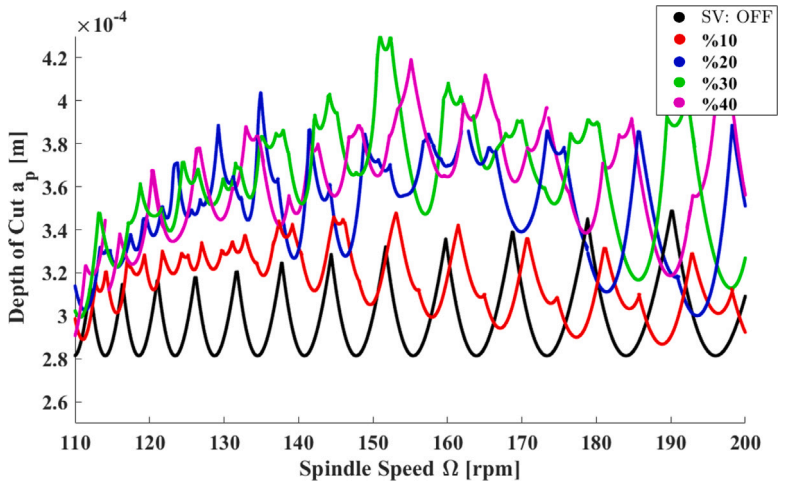

Fig. 17. Sensitivity analysis of stiffness variation amplitude.

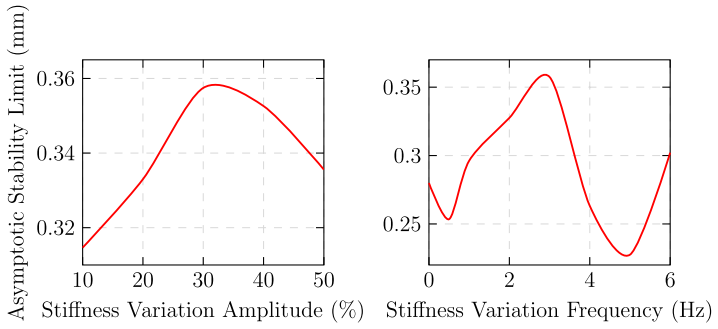

Fig. 18. Trends of asymptotic stability limit.

The results indicate that both the asymptotic and peak stability limits increase as the SV amplitude ratio is increased from 10% to 30%. However, there is no further noticeable stability improvement when the amplitude ratio is increased beyond 30%. Fig. 18 illustrates the trend of the asymptotic stability limit for varying SV amplitude. Comparable patterns in the stability enhancement can be inferred with different SV frequencies despite slightly varying outcomes.

The 3D plot whose axes are SV amplitude, SV frequency, and asymptotic depth of cut was reported in Fig. 19. This plot shows the trend of the stability limit approximately between 130–150 rpm spindle speed range. The plot shows that the maximum performance of chatter suppression with a 28% increase in stability limit is achieved with the parameters of 3 Hz of SV frequency and 20%–30% of SV amplitude. Through sensitivity analysis, it was observed that frequencies that are too low or too high have poor chatter suppression performance. Instead, there exists an optimal SV frequency interval for a specific spindle speed range. It is important to emphasize that the chosen SV amplitude and frequency should reside within a robust region where the slope of the 3D plot is minimal. For instance, if one selects an SV amplitude of 40% and an SV frequency of 6 Hz, it becomes feasible to enhance the stability limit. However, it is noteworthy that the slope of the 3D stability surface is steep in the vicinity of this region, and even slight alterations in SV parameters could lead to a sudden deterioration in chatter suppression performance.

The optimal selection of time-varying amplitude and frequency for SV must consider technological constraints in real-world industrial settings, such as the power limitations of control systems and energy efficiency concerns. These limitations depend on the size of the machine and the method employed to adjust the stiffness of the spindle unit. A brief comparison of various actuation mechanisms based on response time, achievable amplitude ratio, power consumption, and machine scale was presented in Table 5. Generally, smaller-scale machines can attain higher variation frequencies using piezoelectric materials or MR and electrorheological (ER) fluids, which offer swift response times. ER fluids undergo changes in viscosity when subjected to an electric field, distinguishing them for their ability to modulate viscosity. Both ER and MR fluids exhibit rapid adaptability in stiffness adjustment [34]. In contrast, larger machines with mechanical actuation mechanisms may exhibit slower response times, limiting their maximum achievable frequencies. The amplitude of SV is inversely proportional to its frequency due to power constraints within the system. Mechanical actuators, while energy-intensive and imposing substantial strain on motors, offer the potential for achieving higher SV amplitudes, making them more suitable for large-scale machine tools [8]. Therefore, it is crucial to carefully consider the specific industrial application and machine characteristics when determining the appropriate SV amplitude a_{sv} and frequency f_{sv} for optimal

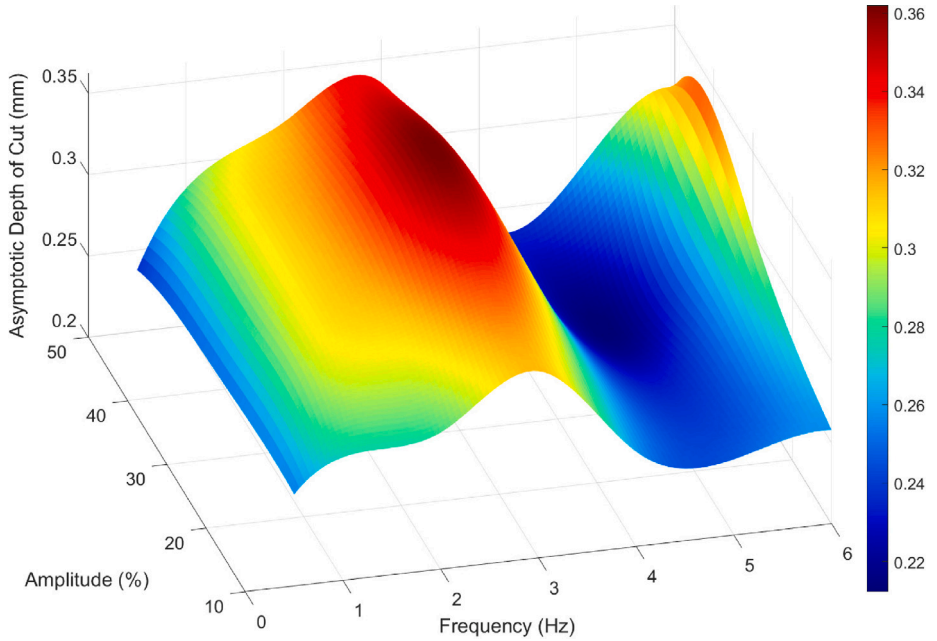

Fig. 19. Sensitivity analysis of stiffness variation amplitude.

Table 5
Comparison of actuator mechanisms for stiffness variation.

Actuation mechanism	Response time	Achievable amplitude ratio	Power consumption	Scale
MR fluids	Low	Low-Moderate	Low-Moderate	Small-Medium
ER fluids	Low	Low-Moderate	Low-Moderate	Small-Medium
Piezoelectric	Moderate	Low-Moderate	Low-Moderate	Small
Relative movement of ram and boring bar	Very high	Very high	Very high	Small-Medium-Large
Hydrostatic bearing with pressure control	High	High	High	Small-Medium-Large

performance. Moreover, practical considerations such as cost, maintenance requirements, and compatibility with existing machine structures should also be taken into account when selecting an actuation mechanism for real-world industrial applications.

4. Conclusions

In summary, this study systematically addressed the intricate challenges posed by the utilization of long and slender boring bars in manufacturing processes, with a specific focus on mitigating static deflection and regenerative chatter. The investigation centers on the efficacy of multi-insert rotating boring bars, deploying cutting inserts in a symmetrical configuration to counterbalance cutting forces and minimize static deflection that leads to higher dimensional accuracy. Simultaneously, the study tackles regenerative chatter by introducing stiffness variation, disturbing the regeneration mechanism, and thereby enhancing the overall stability of boring processes.

The contributions of this research are twofold adapting the multi-dimensional cutting force model to rotating boring bars with multiple inserts and extending the harmonic solution for stability analysis of boring processes with linear-time-periodic dynamics. These advancements deepen the understanding of the complex dynamics of boring processes, offering valuable insights for practitioners and researchers.

The proposed methodology demonstrated its effectiveness through experimental validation, achieving 5 out of 6 matches in stability lobe diagrams for multi-insert rotating boring bars without stiffness variation. Furthermore, the model's comprehensiveness was confirmed by comparing results with existing literature, particularly for single-insert stationary boring bars. Without stiffness variation, the model successfully replicated 4 out of 5 operating points, and with stiffness variation, it accurately predicted all 5 operating points, affirming the robustness of the proposed model for stability analysis in systems exhibiting linear-time-periodic dynamics.

Sensitivity analyses guided the selection of optimal stiffness variation parameters for effective chatter suppression, prioritizing moderate frequencies and up to a 30% amplitude ratio. The result of sensitivity analysis provides guidelines for engineers and machine practitioners in selecting stiffness variation parameters. Avoiding synchronization between tooth passing frequency and stiffness variation frequency is crucial for maintaining optimal chatter suppression performance. Real-world technological

constraints, influenced by machine size and actuation mechanisms, require careful consideration of specific characteristics for achieving optimal performance in industrial applications.

In conclusion, this research establishes a solid theoretical and experimental foundation for the modeling and stability analysis of multi-insert boring bars with stiffness variation. The confirmed effectiveness of stiffness variation and the strategic use of multiple inserts in chatter suppression, as well as the improvement of dimensional accuracy in workpieces, make substantial contributions to the continuous advancement of machining processes.

CRediT authorship contribution statement

Taha Gokulu: Writing – original draft, Validation, Software, Methodology, Formal analysis, Data curation, Conceptualization. **Fabrizio Defant:** Validation, Methodology, Conceptualization. **Paolo Albertelli:** Writing – review & editing, Supervision, Methodology, Conceptualization.

Declaration of competing interest

The authors declare that they have no known competing financial interests or personal relationships that could have appeared to influence the work reported in this paper.

Data availability

Data will be made available on request.

References

[1] W. Takahashi, N. Suzuki, E. Shamoto, Development of a novel boring tool with anisotropic dynamic stiffness to avoid chatter vibration in cutting, Precis. Eng. 68 (2021) 57–71, http://dx.doi.org/10.1016/j.precisioneng.2020.11.007, URL https://linkinghub.elsevier.com/retrieve/pii/S0141635920309831.

[2] B. Tang, H. Akbari, M. Pouya, P.V. Pashaki, Application of piezoelectric patches for chatter suppression in machining processes, Measurement 138 (2019) 225–231, http://dx.doi.org/10.1016/j.measurement.2019.02.003, URL https://linkinghub.elsevier.com/retrieve/pii/S0263224119301137.

[3] B. Yuvaraju, B. Nanda, J. Srinivas, Investigation of stability in internal turning using a boring bar with a passive constrained layer damping, FME Trans. 49 (2021) 384–394, http://dx.doi.org/10.5937/fme2102384Y, URL https://scindeks.ceon.rs/Article.aspx?artid=1451-20922102384Y.

[4] G. Lawrance, P.S. Paul, A.S. Varadarajan, X.A. Vasanth, S.B. Raj, Suppression of tool vibration in boring process: A review, J. Inst. Eng. (India): Ser. C 100 (2019) 1053–1069, http://dx.doi.org/10.1007/s40032-019-00531-z, URL http://link.springer.com/10.1007/s40032-019-00531-z.

[5] M.K. Saleh, M. Nejatpour, H.Y. Acar, I. Lazoglu, A new magnetorheological damper for chatter stability of boring tools, J. Mater. Process. Technol. 289 (2021) 116931, http://dx.doi.org/10.1016/j.jmatprotec.2020.116931, URL https://linkinghub.elsevier.com/retrieve/pii/S0924013620303484.

[6] Y. Altintas, D. Lappin, D. van Zyl, D. Östling, Automatically tuned boring bar system, CIRP Ann 70 (2021) 313–316, http://dx.doi.org/10.1016/j.cirp.2021.04.058, URL https://linkinghub.elsevier.com/retrieve/pii/S0007850621000822.

[7] R.K. Vashisht, Q. Peng, Efficient active chatter mitigation for boring operation by electromagnetic actuator using optimal fractional order PDλ controller, J. Mater. Process. Technol. 276 (2020) 116423, http://dx.doi.org/10.1016/j.jmatprotec.2019.116423, URL https://linkinghub.elsevier.com/retrieve/pii/S0924013619303954.

[8] D. Mei, Z. Yao, T. Kong, Z. Chen, Parameter optimization of time-varying stiffness method for chatter suppression based on magnetorheological fluid-controlled boring bar, Int. J. Adv. Manuf. Technol. 46 (2010) 1071–1083, http://dx.doi.org/10.1007/s00170-009-2166-9, URL http://link.springer.com/10.1007/s00170-009-2166-9.

[9] L. Li, B. Sun, H. Hua, Analysis of the vibration characteristics of a boring bar with a variable stiffness dynamic vibration absorber, Shock Vib. 2019 (2019) 1–13, http://dx.doi.org/10.1155/2019/5284194, URL https://www.hindawi.com/journals/sv/2019/5284194/.

[10] D. Mei, T. Kong, A.J. Shih, Z. Chen, Magnetorheological fluid-controlled boring bar for chatter suppression, J. Mater. Process. Technol. 209 (2009) 1861–1870, http://dx.doi.org/10.1016/j.jmatprotec.2008.04.037, URL https://linkinghub.elsevier.com/retrieve/pii/S0924013608003634.

[11] T. Insperger, G. Stépán, Updated semi-discretization method for periodic delay-differential equations with discrete delay, Internat. J. Numer. Methods Engrg. 61 (2004) 117–141, http://dx.doi.org/10.1002/nme.1061, URL https://onlinelibrary.wiley.com/doi/10.1002/nme.1061.

[12] Y. Ding, L. Zhu, X. Zhang, H. Ding, A full-discretization method for prediction of milling stability, Int. J. Mach. Tools Manuf. 50 (2010) 502–509, http://dx.doi.org/10.1016/j.ijmachtools.2010.01.003, URL https://linkinghub.elsevier.com/retrieve/pii/S089069551000012X.

[13] Y. Sun, Z. Xiong, High-order full-discretization method using Lagrange interpolation for stability analysis of turning processes with stiffness variation, J. Sound Vib. 386 (2017) 50–64, http://dx.doi.org/10.1016/j.jsv.2016.08.039, URL https://linkinghub.elsevier.com/retrieve/pii/S0022460X16304941.

[14] F. Defant, P. Albertelli, A novel harmonic solution for chatter stability of time periodic systems, J. Sound Vib. 490 (2021) 115719, http://dx.doi.org/10.1016/j.jsv.2020.115719, URL https://linkinghub.elsevier.com/retrieve/pii/S0022460X20305496.

[15] N. Wereley, S. Hall, Frequency Response of Linear Time Periodic Systems, vol. 6, IEEE, 1990, pp. 3650–3655, http://dx.doi.org/10.1109/CDC.1990.203516, URL http://ieeexplore.ieee.org/document/203516/.

[16] F. Atabey, I. Lazoglu, Y. Altintas, Mechanics of boring processes—Part II—multi-insert boring heads, Int. J. Mach. Tools Manuf. 43 (2003) 477–484, http://dx.doi.org/10.1016/S0890-6955(02)00277-8, URL https://linkinghub.elsevier.com/retrieve/pii/S0890695502002778.

[17] F. Atabey, I. Lazoglu, Y. Altintas, Mechanics of boring processes—Part I, Int. J. Mach. Tools Manuf. 43 (2003) 463–476, http://dx.doi.org/10.1016/S0890-6955(02)00276-6, URL https://linkinghub.elsevier.com/retrieve/pii/S0890695502002766.

[18] I. Lazoglu, F. Atabey, Y. Altintas, Dynamics of boring processes: Part III-time domain modeling, Int. J. Mach. Tools Manuf. 42 (2002) 1567–1576, http://dx.doi.org/10.1016/S0890-6955(02)00067-6, URL https://linkinghub.elsevier.com/retrieve/pii/S0890695502000676.

[19] E. Budak, E. Ozlu, Analytical modeling of chatter stability in turning and boring operations: A multi-dimensional approach, CIRP Ann 56 (2007) 401–404, http://dx.doi.org/10.1016/j.cirp.2007.05.093, URL https://linkinghub.elsevier.com/retrieve/pii/S0007850607000972.

[20] C.H. Chen, K.W. Wang, Y.C. Shin, An integrated approach toward the dynamic analysis of high-speed spindles: Part I—System model, J. Vib. Acoust. 116 (1994) 506–513, http://dx.doi.org/10.1115/1.2930456, URL https://asmedigitalcollection.asme.org/vibrationacoustics/article/116/4/506/441533/An-Integrated-Approach-Toward-the-Dynamic-Analysis.

[21] C.-J. Li, A.G. Ulsoy, W.J. Endres, The effect of flexible-tool rotation on regenerative instability in machining, J. Manuf. Sci. Eng. 125 (2003) 39–47, http://dx.doi.org/10.1115/1.1536657, URL https://asmedigitalcollection.asme.org/manufacturingscience/article/125/1/39/445973/The-Effect-of-FlexibleTool-Rotation-on.

[22] G. Wang, H. Dong, Y. Guo, Y. Ke, Chatter mechanism and stability analysis of robotic boring, Int. J. Adv. Manuf. Technol. 91 (2017) 411–421, http://dx.doi.org/10.1007/s00170-016-9731-9, URL http://link.springer.com/10.1007/s00170-016-9731-9.
[23] T.L. Schmitz, K.S. Smith, Machining Dynamics, Springer International Publishing, Cham, 2019, http://dx.doi.org/10.1007/978-3-319-93707-6, URL http://link.springer.com/10.1007/978-3-319-93707-6.
[24] Y. Altintaş, E. Budak, Analytical prediction of stability lobes in milling, CIRP Ann 44 (1995) 357–362, http://dx.doi.org/10.1016/S0007-8506(07)62342-7, URL https://linkinghub.elsevier.com/retrieve/pii/S0007850607623427.
[25] Y. Altintas, Manufacturing Automation, Cambridge University Press, 2012, http://dx.doi.org/10.1017/CBO9780511843723, URL https://www.cambridge.org/core/product/identifier/9780511843723/type/book.
[26] C. Mei, Active regenerative chatter suppression during boring manufacturing process, Robot. Comput.-Integr. Manuf. 21 (2005) 153–158, http://dx.doi.org/10.1016/j.rcim.2004.07.011, URL https://linkinghub.elsevier.com/retrieve/pii/S0736584504000742.
[27] M. Wang, R. Fei, Chatter suppression based on nonlinear vibration characteristic of electrorheological fluids, Int. J. Mach. Tools Manuf. 39 (1999) 1925–1934, http://dx.doi.org/10.1016/S0890-6955(99)00039-5, URL https://linkinghub.elsevier.com/retrieve/pii/S0890695599000395.
[28] C. Wang, X. Zhang, Y. Liu, H. Cao, X. Chen, Stiffness variation method for milling chatter suppression via piezoelectric stack actuators, Int. J. Mach. Tools Manuf. 124 (2018) 53–66, http://dx.doi.org/10.1016/j.ijmachtools.2017.10.002, URL https://www.sciencedirect.com/science/article/pii/S0890695517301414.
[29] E. Möllerstedt, Dynamic Analysis of Harmonics in Electrical Systems (Ph.D. thesis), Lund Institute of Technology, 2000.
[30] D. Bachrathy, G. Stépán, Bisection method in higher dimensions and the efficiency number, Period. Polytech. Mech. Eng. 56 (2012) 81, http://dx.doi.org/10.3311/pp.me.2012-2.01, URL https://pp.bme.hu/me/article/view/1236.
[31] T.G. Molnar, T. Insperger, G. Stepan, Closed-form estimations of the bistable region in metal cutting via the method of averaging, Int. J. Non-Linear Mech. 112 (2019) 49–56, http://dx.doi.org/10.1016/j.ijnonlinmec.2018.09.005.
[32] D. Hajdu, T. Insperger, G. Stepan, Quantification of uncertainty in machining operations based on probabilistic and robust approaches, 77, Elsevier B.V., 2018, pp. 82–85, http://dx.doi.org/10.1016/j.procir.2018.08.226,
[33] F. DEFANT, Stiffness variation development to suppress chatter vibration in large boring machines and study of its potentiality with other chatter avoidance strategies, 2023, URL https://www.politesi.polimi.it/handle/10589/196742?mode=complete.
[34] I. Chopra, in: I. Chopra, J. Sirohi (Eds.), Electrorheological and Magnetorheological Fluids, Cambridge University Press, Cambridge, 2013, pp. 685–738, http://dx.doi.org/10.1017/CBO9781139025164.008, URL https://www.cambridge.org/core/product/8D4836D77EA34853D3C4D8D813F61E40.